Cerium intermetallics with ZrNiAl-type structure - a review

Rainer Pöttgen, Bernard Chevalier

Review

Rainer Pöttgen* and Bernard Chevalier

Cerium intermetallics with ZrNiAl-type structure – a review

Abstract: Equiatomic Ce*TX* intermetallics with the hexagonal ZrNiAl type structure are formed with electron-rich transition metals (*T*) and *X* = Mg, Zn, Cd, Al, Ga, In, Tl, Sn, and Pb. Their crystal chemistry, chemical bonding, magnetic and electrical properties, and formation of solid solutions are reviewed. The results of ^{119}Sn Mössbauer spectroscopy, high-pressure studies, and hydrogenation reactions are presented.

Keywords: cerium compounds; crystal structure; intermetallics; magnetic properties; structure-property relationship.

DOI 10.1515/znb-2015-0018
Received February 2, 2015; accepted February 12, 2015

1 Introduction

In the large field of rare earth (*RE*) based intermetallic compounds [1] those of cerium have attracted broad interest among solid state chemists and physicists with respect to their crystal chemistry and physical properties. Cerium can adopt two different valence states, diamagnetic Ce^{4+} with [Xe] configuration and paramagnetic Ce^{3+} with [Xe]$4f^1$ configuration. Many cerium compounds have been studied in the framework of strongly correlated electron systems [2–8]. Striking materials properties have been observed in the field of Kondo compounds, antiferromagnetic and ferromagnetic ordering, valence fluctuation, heavy fermion compounds, superconductivity, or non-Fermi liquid systems.

***Corresponding author: Rainer Pöttgen,** Institut für Anorganische und Analytische Chemie, Universität Münster, Corrensstrasse 30, 48149 Münster, Germany, e-mail: pottgen@uni-muenster.de
Bernard Chevalier: Institut de Chimie de la Matière Condensée de Bordeaux, CNRS, Université Bordeaux, ICMCB, UPR 9048, F-33600 Pessac, France

As an exceptional class of cerium intermetallics, the equiatomic Ce*TX* compounds (*T* = electron-rich transition metal; *X* = element of the 3rd, 4th, or 5th main group) have intensively been studied within the last thirty years [1, 9, 10]. Most of them crystallize with simple structure types (space group symbols in parentheses), *viz*. TiNiSi (*Pnma*), ZrNiAl ($P\bar{6}2m$), ZrBeSi ($P6_3/mmc$), NdPtSb ($P6_3mc$), PbFCl ($P4/nmm$), or LaPtSi ($I4_1md$) with single crystallographic cerium sites. The manifold of magnetic properties in the Ce*TX* compounds is a consequence of crystal field effects and the course of the hybridization of the Ce(4*f*) electrons with the conduction electrons. These two mechanisms can disturb localization of the *f* electrons, leading to an itinerant renormalized state near the Fermi level. These non-fully localized *f* states cause the anomalous magnetic and electrical properties of Ce*TX* intermetallics. The electronic situation at the Ce atoms can experimentally be changed through different parameters: (i) formation of solid solutions through partial substitution of *T* or *X*, (ii) change of the valence electron count through complete substitution of *T* or *X* with another *d* or *p* group element, (iii) dilution of the Ce(4*f*) moments through partial Ce/La substitution, (iv) application of pressure, or (v) hydrogenation reactions.

In the present review we focus on the group of Ce*TX* intermetallics with ZrNiAl type structure. Their crystal chemical details and chemical bonding peculiarities are discussed along with magnetic and transport data in order to elucidate structure-property relationships.

2 Synthesis conditions

Most of the Ce*TX* samples can be prepared directly from the pure elements via arc-melting [11] under purified argon. Such samples are usually re-melted several times to ensure homogeneity, followed by long-term annealing sequences (typically at 1070 K) in sealed silica ampoules in tube or muffle furnaces. For the growth of small crystals for structure determination very slow cooling rates are desirable. For some indides, an addition of up to 3

weight-percent indium has been used for compensation of the loss via evaporation during the arc-melting procedure.

For elements with comparatively low boiling temperatures, e.g., Mg, Zn, Cd, and Tl, synthesis via arc-melting would result in enormous weight losses due to evaporation. To give an example, in the synthesis of CePtMg [12], magnesium already boils (1363 K) before platinum melts (2045 K) [13]. Such samples need to be prepared in sealed high-melting metal ampoules, mostly niobium or tantalum [11, 14, 15]. The thermal treatment can be performed in muffle or tube furnaces (with an additional silica ampoule for oxidation protection) or under argon atmosphere in induction furnaces [16, 17]. CeIrIn [18] was also synthesized in a tantalum ampoule with an addition of 5 at.-% indium for flux growth conditions [19].

Most studies of the Ce*TX* phases were performed on polycrystalline samples prepared by arc-melting. Orientation dependent physical property measurements are only possible with larger single crystals. These are obtained from a metal flux [19]; e.g., large CePtPb crystals were grown from molten lead and the crystals were separated by centrifugation [20]. Another standard crystal growth technique is the Czochralski method, starting from arc-melted polycrystalline samples in a tri-arc furnace. This technique has been used for the growth of CeNiIn, CeRhIn, and CePdIn crystals [21–24]. A special situation occurred for CePtIn. Czochralski growth of this indide led to indium evaporation, and better results were obtained by the floating zone method in a four-mirror optical furnace [25, 26].

High-pressure high-temperature Ce*T*Sn phases have been prepared in a multianvil assembly [27–30] using boron nitride as inner crucible material. Arc-melted and carefully grinded Ce*T*Sn normal-pressure phases (*T* = Ni, Pd, Pt [31–33]) were loaded into the assemblies and treated under maximum pressure and temperature conditions of 11.5 GPa and 1470 K. For details we refer to the original articles.

An important synthetic aspect concerns hydrogenation reactions of Ce*TX* intermetallics aiming at modifications of the physical properties [34–38]. Such hydrogenation reactions start directly from the arc-melted samples which are mostly activated under vacuum at higher temperature prior to hydrogen uptake. The hydrogenation is then carried out either at room temperature or at slightly elevated temperature. Hydrogen pressures up to ca. 50 bars have been applied. Often the hydrides are cycled several times to ensure homogeneity of the sample. The amount of absorbed hydrogen can be estimated from pressure changes in a calibrated volume. Hydrogen uptake mostly leads to complete crumbling of the sample. Several groups have treated the sample surfaces with carbon disulfide (surface poisoning) in order to prevent any loss of hydrogen. Samples for neutron powder diffraction are prepared with deuterium instead of hydrogen. The kinetics is monitored through hydrogen absorption isotherms. The initial hydrogen uptake of such intermetallic samples is often slow; a consequence of surface passivation. For the concrete experimental hydrogenation parameters we refer to the original papers.

3 Discussion

3.1 Crystal chemistry and chemical bonding

More than 30 intermetallic cerium compounds Ce*TX* crystallize with the hexagonal ZrNiAl type structure [54, 80, 81], space group $P\bar{6}2m$, Pearson symbol hP9, and Wyckoff sequence *gfda*. The basic crystallographic data of these phases are listed in Table 1. The ZrNiAl structure itself can be considered as a ternary ordered version of the Fe_2P type [82]. The basic crystal chemistry of the ZrNiAl phases (the Pearson data base [1] lists more than 1700 entries for this structure type) is well documented [2, 83, 84]. Herein we focus only on the peculiarities of the cerium containing materials.

The Ce*TX* phases show broad coloring on the *T* and *X* sites, i.e., *T* = Ni, Cu, Rh, Pd, Ag, Ir, Pt, and Au and *X* = Mg, Zn, Cd, Hg, Al, Ga, In, Tl, Sn, and Pb, leading to a large structural flexibility. These colorings offer valence electron counts between 14 (CeRhMg) and 17 (CeAuIn). Three further phases show the same atomic sites, but a coloring exclusively with *p* elements. In the structures of CeMg*X* (*X* = Ga, In, Tl) [39–42], the *p* element takes the position of the transition metals, leading to a different bonding pattern.

As an example we present the CeRhSn structure in Fig. 1. Ce atoms fill Wyckoff site 3*f* (*x* 0 0) with *x* = 0.41444, the two crystallographically independent rhodium sites are 2*d* (1/3 2/3 1/2) (Rh1) and 1*a* (0 0 0) (Rh2), and the Sn atoms are on 3*g* (*x* 0 1/2) with *x* = 0.75012. The striking structural motif is the trigonal prismatic coordination of the Rh atoms. Rh1 has six cerium neighbors at 304 pm Rh1–Ce and the Rh2 has six tin neighbors at 277 pm Rh2–Sn. The Rh1@Ce_6 prisms are condensed via common edges in *ab* direction forming six-membered rings which further condense in *c* direction via common triangular faces. This substructure leaves large channels which are filled by rows of Rh2@Sn_6 prisms. Both prismatic substructures are shifted with respect to each other by half the lattice parameter *c*. This leads to coordination number 9 for both Rh atoms in the form of tri-capped trigonal prisms (Fig. 2),

Table 1: Lattice parameters of CeMg*X* and Ce*TX* phases with hexagonal ZrNiAl type structure.

Compound	*a* (pm)	*c* (pm)	*c*/*a*	*V* (nm³)	Magnetic behavior	References
p element compounds						
CeMgGa	752.7(2)	454.8(1)	0.604	0.2232	T_N = 3.1 K	[39, 40]
CeMgIn	774.9(3)	477.7(2)	0.616	0.2484	n.i.	[41]
CeMgTl	774.1(1)	473.75(7)	0.612	0.2458	n.i.	[42]
d element compounds						
$CeRh_{1.262}Mg_{0.738}$	752.3(1)	417.6(1)	0.555	0.2047	n.i.	[43]
CePdMg	767.3(1)	410.37(4)	0.535	0.2092	T_N = 2.1 K	[12]
CePdMg	765.1(1)	410.3(1)	0.536	0.2080	n.i.	[44]
CePdMg	760	408	0.537	0.2041	< 2 K	[45]
CeAgMg	782.5(3)	432.8(1)	0.553	0.2295	< 2 K	[46, 47]
CeAgMg	782.3(2)	433.1(1)	0.554	0.2295	n.i.	[44]
CePtMg	755.02(7)	413.82(4)	0.548	0.2043	T_N = 3.6 K	[12]
CeAuMg	774.1(3)	421.6(1)	0.545	0.2188	T_N = 2.0 K	[12]
CeNiZn	713.3(3)	388.7(1)	0.545	0.1713	IV	[48]
CeNiZn	714.1(1)	388.8(1)	0.544	0.1717	n.i.	[49]
α-CePdZn	739.9(1)	401.4(1)	0.543	0.1903	n.i.	[49]
α-CePdZn	740.4(1)	402.18(5)	0.543	0.1909	< 2 K	[50]
CeCuCd	759.6(2)	411.6(2)	0.542	0.2057	n.i.	[49]
CePdCd	767.7(1)	405.8(1)	0.529	0.2066	n.i.	[49]
CePdCd	768.1(2)	406.37(8)	0.529	0.2076	n.i.	[51]
CePtCd	763.8(6)	409.1(4)	0.536	0.2067	n.i.	[53]
CeAuCd	782.91(9)	410.01(5)	0.524	0.2176	n.i.	[52]
CeAuCd	783.2(2)	410.67(9)	0.524	0.2182	T_N = 3.7 K	[53]
CeNiAl	697.56(4)	402.06(3)	0.576	0.1694	n.i.	[54]
CeNiAl	697.60(5)	401.87(5)	0.576	0.1694	IV	[55]
CeNiAl	697.7	399.8	0.573	0.1685	n.i.	[101]
CeCuAl	717.6(4)	419.8(3)	0.585	0.1872	n.i.	[54]
CeCuAl	717.9	420.1	0.585	0.1875	n.i.	[101]
CeCuAl	717.7(3)	420.8(2)	0.586	0.1877	< 5 K	[102]
CeCuAl	718.3	420.8	0.586	0.1880	T_N = 5.2 K	[103]
CePdAl	721.98(7)	423.29(7)	0.586	0.1911	n.i.	[56]
CePdAl	721.7(2)	423.1(1)	0.586	0.1908	n.i.	[57]
α-CeNiGa	694.6(7)	398.7(4)	0.574	0.1666	n.i.	[58]
α-CeNiGa	695.07(1)	397.89(1)	0.572	0.1665	IV	[37]
$CeNiGa_{0.5}Al_{0.5}$	697.48(8)	402.41(5)	0.577	0.1695	n.i.	[37]
CeNiIn	752.0(1)	397.34(8)	0.528	0.1946	n.i.	[59]
CeNiIn	752.0	397.2	0.528	0.1945	IV	[38]
CeNiIn	754.02(7)	397.99(6)	0.528	0.1960	n.i.	[60]
CeNiIn	753.4(1)	397.5(1)	0.528	0.1954	n.i.	[61]
CeCuIn	749.15(6)	424.52(5)	0.567	0.2063	< 1.9 K	[62]
CeCuIn	749.2(2)	424.52(15)	0.567	0.2064	n.i.	[59]
CeCuIn	749.15(18)	424.52(15)	0.567	0.2063	n.i.	[63]
CeRhIn	754.7	405	0.537	0.1998	IV	[64]
CeRhIn	755.2	405.5	0.537	0.2003	IV	[65]
CeRhIn	755.5	405.5	0.537	0.2004	n.i.	[100]
CePdIn	770.36(15)	401.90(14)	0.522	0.2066	n.i.	[66]
CePdIn	770.03(4)	407.41(3)	0.529	0.2094	< 2 K	[67]
CePdIn	770.03(4)	407.41(3)	0.529	0.2092	n.i.	[59]
CePdIn	769.8	407.6	0.529	0.2092	T_N = 1.65 K	[68]
CePdIn	768.6(2)	406.7(1)	0.529	0.2081	< 1.8 K	[69]
CeIrIn	757.8(2)	405.63(7)	0.535	0.2017	n.i.	[18]
CePtIn	765.4(2)	407.1(1)	0.532	0.2065	< 0.4 K	[26]
CePtIn	765.3(2)	406.8(1)	0.532	0.2063	< 2 K	[70]
CePtIn	770.6(1)	409.7(1)	0.532	0.2107	n.i.	[71]
CePtIn	765.7	406.9	0.531	0.2066	n.i.	[100]
CeAuIn	769.8(2)	425.6(1)	0.553	0.2184	n.i.	[72]
CeAuIn	768.8(1)	426.2(1)	0.554	0.2182	n.i.	[59]

(Table 1: Continued)

Compound	*a* (pm)	*c* (pm)	*c*/*a*	*V* (nm³)	Magnetic behavior	References
CePdTl	784.0(2)	396.3(1)	0.505	0.2110	n.i.	[73]
HP-CeNiSn	744.6(2)	406.39(9)	0.546	0.1951	n.i.	[31]
CeRhSn	744.8(2)	408.00(9)	0.548	0.1960	IV	[74]
CeRhSn	745.8(1)	408.62(9)	0.548	0.1968	n.i.	[75]
CeRhSn	755	397	0.526	0.1960	IV	[104]
HP-CePdSn	760.03(5)	416.06(3)	0.547	0.2081	T_N = 5 K	[32]
CeIrSn	743.8(2)	407.58(7)	0.548	0.1953	IV	[74]
CeIrSn	744.9(4)	408.0(2)	0.548	0.1953	n.i.	[76]
HP-CePtSn	756.919(5)	415.166(4)	0.548	0.2060	< 2 K	[33]
CeRhPb	767.1(1)	402.74(7)	0.525	0.2052	PP	[77]
CePdPb	775.0(2)	413.32(8)	0.533	0.2150	< 3 K	[78]
CePdPb	775.0(5)	414.0(4)	0.534	0.2153	n.i.	[44]
CePdPb	774.2	413.8	0.534	0.2148	n.i.	[79]
CePtPb	774	413	0.534	0.2143	T_N = 0.9 K	[20]
CePdHg	772.8(5)	395.3(3)	0.512	0.2045	n.i.	[44]

IV, intermediate valence; T_N, Néel temperature; n.i., not investigated. For samples that did not show magnetic ordering the lowest measuring temperature is given.

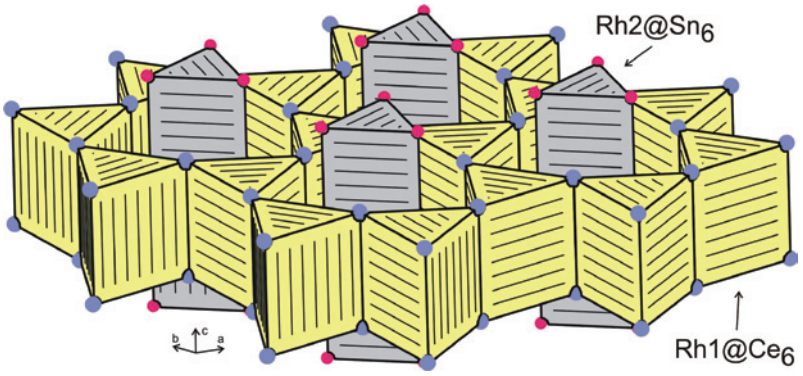

Fig. 1: The crystal structure of CeRhSn [75]. Cerium and tin atoms are drawn as blue and magenta circles, respectively. The trigonal prisms around the two crystallographically independent rhodium atoms are emphasized.

a typical coordination in intermetallic compounds [15]. The high structural flexibility of this structural arrangement relies on the easy adjustment of the size of the two trigonal prisms (*c*/*a* ratio) through changes of the lattice parameters and the two *x* parameters.

The shortest interatomic distances in the CeRhSn structure occur for Rh–Sn (277 and 285 pm), only slightly longer than the sum of the covalent radii of 265 for Rh + Sn [13]. One can thus assume significant Rh–Sn bonding and the formation of a three-dimensional polyanionic $[RhSn]^{\delta-}$ network (Fig. 3), in agreement with electronic structure calculations [9, 75]. The triangular faces of the $Rh2@Sn_6$ prisms show Sn–Sn distances of 323 pm, close to the Sn–Sn distances in metallic β-Sn (4 × 302 and 2 × 318 pm) [85]. Besides covalent Rh–Sn bonding, the $[RhSn]^{\delta-}$ network is additionally stabilized through Sn–Sn bonding interactions.

Ce atoms have five Rh atoms as closest neighbors with Ce–Rh distances of 304 and 309 pm, slightly longer than the sum of the covalent radii for Ce + Rh of 290 pm [13]. These bonding interactions are a direct consequence of

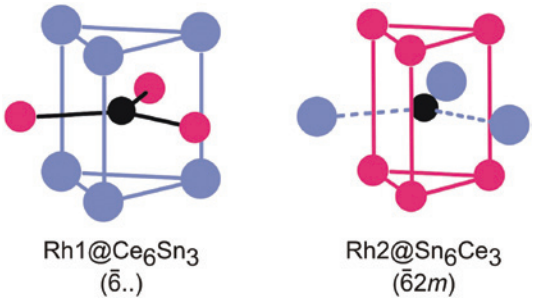

Fig. 2: Coordination of the two rhodium atoms in CeRhSn. The site symmetries are indicated.

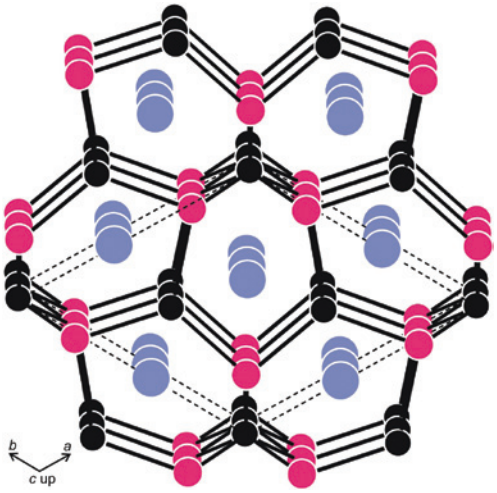

Fig. 3: The structure of CeRhSn. Cerium, rhodium, and tin atoms are drawn as blue, black, and magenta circles, respectively. The three-dimensional $[RhSn]^{\delta-}$ polyanionic network is emphasized.

the course of the electronegativities, rhodium being more electronegative than tin. Electronic structure calculations showed remarkable covalent Ce–Rh bonding. These bonds play an important role for the physical properties of CeRhSn (*vide infra*). The near-neighbor coordination of the Ce atoms in CeRhSn is presented in Fig. 4. Each Ce atom has a sandwich-like coordination by two slightly distorted but planar Rh_2Sn_3 pentagons which are connected through a common Rh atom. Within the *ab* plane there are four cerium neighbors at 389 pm and two further cerium neighbors at 409 pm above and below (the *c* lattice parameter).

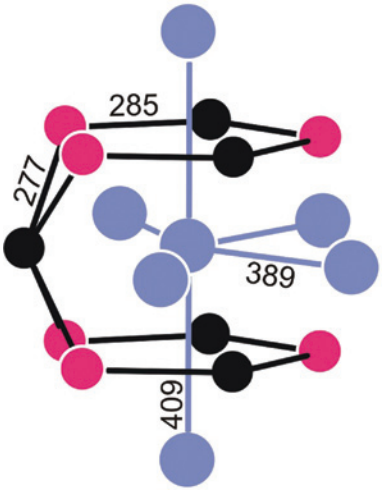

Fig. 4: Coordination of the cerium atoms in CeRhSn. Cerium, rhodium, and tin atoms are drawn as blue, black, and magenta circles, respectively. Relevant interatomic distances (in units of pm) are given.

The Ce–Ce and Ce–*T* distances are important parameters for the magnetic ground state of the Ce*TX* compounds. For those compounds where structure refinements based on powder or single crystal X-ray diffraction data are available we list the corresponding Ce–Ce and Ce–*T* distances in Table 2. For the whole series of Ce*TX* intermetallics the Ce–Ce distances range from 359 to 433 pm. For comparison, the Ce–Ce distance in *fcc* cerium [85] is 365 pm. Furthermore, all Ce–Ce distances in the Ce*TX* phases are longer than the Hill limit of 340 pm for 4*f* electron localization [86]. This will be discussed further along with the magnetic data (*vide infra*). Also the Ce–*T* distances play an important role for the magnetic behavior. For the series of Ce*TX* compounds the Ce–*T* distances range from 288 to 325 pm (Table 2). The course of these distances is primarily a consequence of the size of the transition metal atom. In all cases (for electrostatic reasons), the more electronegative transition metal is the nearest neighbor for the Ce atom. This is also the case for the three triel compounds CeMg*X* (*X* = Ga, In, Tl), which can be considered as a gallide, indide, and thallide. These phases can be taken as *p* element analogs of CeMg*T* (*T* = Rh, Pd, Ag, Pt, Au) which carry a partial negative charge on the *T* atoms [87, 88].

Experimental data on the electronic structures of Ce*TX* intermetallics were obtained from XPS measurements.

Table 2: Ce–Ce and Ce–*T* distances for the Ce*TX* compounds where the structures were refined from single crystal or powder diffraction data.

Compound	Ce–Ce (pm)	Ce–*T* (pm)	References
$CeRh_{1.262}Mg_{0.738}$	392, 418	308, 313	[43]
CePdMg	399, 410	309, 320	[12]
CeAgMg	408, 433	320, 325	[46]
CePtMg	394, 414	307, 313	[12]
CeAuMg	404, 422	314, 321	[12]
CeNiZn	372, 389	290, 297	[48]
α-CePdZn	387, 402	301, 305	[50]
CeAuCd	410, 411	314, 320	[52]
CeNiAl	362, 402	290, 293	[54]
CePdAl	374, 423	303, 304	[56]
α-CeNiGa	359, 399	288, 295	[58]
CeNiIn	394, 397	302, 308	[59]
CeCuIn	390, 425	309, 312	[63]
CePdIn	402, 402	307, 318	[66]
CeIrIn	397, 406	306, 311	[18]
CePtIn	400, 407	308, 316	[70]
CeAuIn	403, 426	314, 316	[59]
CeRhSn	389, 409	304, 309	[75]
HP-CePdSn	397, 416	310, 314	[32]
CeIrSn	388, 408	303, 308	[74]
HP-CePtSn	395, 415	309, 313	[33]
CeRhPb	402, 403	307, 314	[77]

These experiments gave direct evidence for the location of the Ce(4*f*) and *T*(n*d*) levels with respect to the Fermi level. Detailed studies were performed for the indides Ce*T*In (*T* = Ni, Cu, Pd, Pt, Au) [59, 62, 67, 71]. The XPS spectra clearly confirm the intermediate cerium valence in CeCuIn [62]. For CeRhIn and CeRhSn high-resolution photoemission studies have revealed a strong Ce($4f^1$) contribution near the Fermi level. Together with a weak Ce($4f^0$) peak this indicates strong valence fluctuations in both compounds, but with a weaker hybridization strength in CeRhSn [89].

Not all ZrNiAl type Ce*TX* compounds are stable over the whole temperature range. The gallide CeNiGa [90, 91] and the zinc compound CePdZn [50] transform to TiNiSi type high-temperature modifications. In the case of CePdZn, electronic structure calculations along with magnetic data point to larger Ce(4*f*)–Pd(4*d*) hybridization for the ZrNiAl type phase.

3.2 Magnetic properties

The intermetallic Ce*TX* compounds belong to the class of strongly correlated electron systems. The main parameter that governs the broadly varying physical properties is the coupling constant J_{cf} between the Ce(4f) and the conduction electrons. One can then observe competition between the well-known indirect RKKY interactions [92–94] and the Kondo effect [95, 96]. The interplay of these parameters has qualitatively been described in the Doniach diagram [97] and its updated versions [2, 98, 99]. Based on this scheme on can roughly regroup the cerium compounds into three classes, i.e., (i) a normal localized Ce(4*f*) state along with a magnetic moment (called a magnetic RKKY metal) occurs if the Ce(4*f*) level lies below the Fermi level, (ii) a magnetic Kondo system, when the Ce(4*f*) level approaches the Fermi level, leading to a reduction of the magnetic ordering temperature and the magnetic moment, and (iii) a non-magnetic Kondo system in the case of a further increase of J_{cf}, leading to valence fluctuations. Some correlation of the magnetic properties of the Ce*TX* intermetallics with the interatomic distances and the cell volume has been observed. Besides these general parameters influencing the Ce(4*f*) states, the triangular arrangement of the Ce atoms (slightly distorted Kagomé network) in the ZrNiAl type can cause topological frustration of the Ce(4*f*) moments. This will be discussed in more detail along with the magnetic structures determined from neutron diffraction data (*vide infra*). In the following discussion we start with the materials of the first group which show magnetic ordering. As is evident from Table 1, the Néel temperatures are low in all cases.

All Ce*TX* compounds with trivalent cerium show experimental effective magnetic moments close to the free ion value of 2.54 μ_B for Ce^{3+}. As a first example we present the ternary gallide CeMgGa which orders antiferromagnetically at T_N = 3.1 K [39] and shows a metamagnetic transition at a critical field strength of 1 *T*. In the magnetically ordered state, the magnetic moment at 5 T and 1.72 K of 0.8 μ_B per cerium atom is significantly reduced when compared with the theoretical value of 2.14 μ_B according to $g \times J$, frequently observed in many cerium based intermetallics.

The high-pressure modifications HP-CePdSn [32] and HP-CePtSn [33] also show stable trivalent cerium over the whole temperature range. Low-field magnetic susceptibility and specific heat data point to antiferromagnetic ordering at T_N = 5 K for the palladium compound, while HP-CePtSn remains paramagnetic down to 2 K. In comparison with the TiNiSi type normal-pressure modification of CePdSn one observes a decrease of the magnetic ordering temperature from 7.5 to 5 K.

The magnesium compounds CePdMg, CePtMg, and CeAuMg [12, 45] show Curie-Weiss behavior and negative paramagnetic Curie temperatures of –36, –35, and –57 K, respectively, hinting to antiferromagnetic interactions in the paramagnetic range. Low-field susceptibility measurements have shown antiferromagnetic ordering at T_N = 2.1, 3.6, and 2.0 K for CePdMg, CePtMg, and CeAuMg, respectively, and this was confirmed through specific heat measurements. The isotypic silver compound CeAgMg is also trivalent with 2.52 μ_B per Ce atom; however, no magnetic ordering occurs down to 2 K [47]. When substituting magnesium by cadmium one obtains the isoelectronic compound CeAuCd which orders antiferromagnetically at T_N = 3.7 K [53]. This increase is most likely not due to geometrical parameters, since the unit cells of both gold compounds are very similar (Table 1).

The aluminide CeCuAl (T_N = 5.2 K) has one of the highest Néel temperatures in the series of Ce*TX* compounds [102, 103, 105]. A curvature in the temperature dependence of the magnetic susceptibility at low temperatures is indicative of the presence of crystal field effects. The trivalent ground state of cerium in CeCuAl has been confirmed by core-level spectroscopy [105]. An important issue regarding the investigated CeCuAl samples concerns ferromagnetic impurity phases which can affect the susceptibility measurements. The isotypic indide CeCuIn does not order magnetically down to 1.9 K [62, 63]. Nevertheless, cerium is in a stable trivalent ground state with an experimental effective magnetic moment of 2.50 μ_B per cerium atom. This is underlined by XPS spectra which also show some hybridization of the Ce(4*f*) states with the conduction band states.

The so far highest Néel temperature in this structural family has been measured for CeAuIn (T_N = 6 K) [106–108]. The magnetic structure determination of CeAuIn was based on neutron powder diffraction data. CeAuIn is a simple antiferromagnet with a propagation vector **k** = (0, 0, 1/2) and an absolute value of the cerium magnetic moment (lying within the *ab* plane) of 1.2 μ_B.

The magnetic behavior of CePdAl has been studied in detail on powder samples as well as on single crystals grown by the Czochralski method [109, 110]. A partially ordered antiferromagnetic ground state has been observed below T_N = 2.7 K. The main interest of these investigations concerned frustration of the cerium magnetic moments, a consequence of the Kagomé-related arrangement of the Ce atoms. Besides the susceptibility and heat capacity studies also theoretical investigations were performed. The thermodynamic properties of CePdAl were evaluated along with orbital degeneracy and crystal field effects. Approval of the model was obtained through fits of the specific heat data [111]. The heavy fermion character of CePdAl was evidenced from C_P data which revealed an electronic specific heat coefficient of $\gamma \approx 610$ mJ mol^{-1} K^{-2} [112]. Electronic structure calculations along with XPS core level and valence band spectra show strong hybridization of the Ce(4*f*) and Pd(4*d*) states, strongly influencing the magnetic ground state properties of CePdAl [113]. The crystal electric field (CEF) levels of ≈ 240 K and > 400 K were determined from inelastic neutron scattering experiments. The energies of the CEF excitations are E_1 = 21.09 and E_2 = 44.7 meV [114].

The geometrical magnetic frustration in CePdAl was thoroughly studied by neutron diffraction [115–117]. The alignment of the cerium magnetic moments is not as simple as in CeAuIn discussed above. The diffraction data showed an incommensurate antiferromagnetic propagation vector **k** = (1/2, 0, 0.35), leading to a longitudinal sine-wave modulated arrangement of the spins. Within this spin structure, magnetically ordered moments coexist with frustrated, disordered moments. In total, only 2/3 of the cerium magnetic moments are in an ordered state with moments of 1.6–1.8 μ_B. Additional neutron diffraction experiments on a CePdAl single crystal under an applied magnetic field of 5.5 T along the easy axis of magnetization (*c* axis) show a hysteretic process. Those moments that are geometrically frustrated under zero-field conditions can be lifted under the influence of the applied field [117].

^{27}Al solid state NMR spectroscopic data on polycrystalline CePdAl samples are indicative of a slow spin fluctuation rate below the Néel temperature [109, 118, 119]. Spin-echo spectra are compatible with the partially ordered magnetic state derived from the neutron diffraction experiments.

The stability of the partial antiferromagnetic ground state of CePdAl was tested under high magnetic field and high-pressure conditions [120–123]. Magnetization experiments were carried out up to an external field strength of 43 T. CePdAl shows three filed-induced transitions at critical field values of 3.2, 3.4 and 4.0 T and a saturation magnetic moment of 1.05 μ_B at 1.75 K and 43 T, significantly reduced when compared with the theoretical value of 2.14 μ_B, indicating substantial crystal field splitting of the J = 5/2 ground state. Resistivity measurements under high-pressure show disappearance of the magnetic ordering at pressures above 1 GPa.

Now we turn to the compounds with reduced magnetic ordering temperature. Strong Ce(4*f*)-Pd(4*d*) hybridization has been substantiated from electronic structure calculations for α-CePdZn [50]. This low-temperature modification contains stable trivalent cerium (μ_{eff} = 2.42 μ_B), but no magnetic ordering was evident down to 2 K. The plumbides CePdPb and CePtPb show similar behavior. Susceptibility and specific heat studies gave no hint for magnetic ordering of CePdPb down to 3 K [78]. CePtPb [20] orders antiferromagnetically at T_N = 0.9 K and a magnetization isotherm at 2.3 K shows a saturation value of 0.92 μ_B per Ce atom (perpendicular to the *c* axis) at 18 T. Pressure-dependent ac susceptibility measurements show an almost linear increase of the Néel temperature with increasing pressure with a value of 1.2 K at 17 kbar. The physical property measurements on a single crystal point to strongly anisotropic behavior which has its origin in the low symmetry CEF at the cerium site within the distorted Kagomé-like networks in the ZrNiAl-type structure.

Broad studies on polycrystalline material as well as for single crystals were reported for the dense Kondo compound CePdIn [23, 68, 124–129]. CePdIn orders antiferromagnetically at T_N = 1.65 K and the heavy fermion ground state was derived from specific heat data. The specific resistivity exhibits a pronounced Kondo minimum around 20 K. Well resolved specific heat studies down to the mK regime reveal a two peak structure for the lambda transition with maxima at 1.7 and 0.9 K [126]. The transition at 1.7 K was attributed to the onset of antiferromagnetic ordering, and the second one to a reorganization of the localized Ce(4*f*) moments. Another possibility is a competition between the antiferromagnetic ordering and formation of a heavy fermion state [128]. The anisotropy of the magnetic behavior was evident from single crystal data, similar to CePtPb [20]. The paramagnetic Curie temperatures along the *a* and *c* axis of −65 and −43 K show distinct

differences and the kink at the Néel point is only visible for the data along *c* [127].

The Debye temperature of CePdIn is 190.7 K and the Ce^{3+} $^2F_{5/2}$ ground state multiplet splits into three Kramers doublets at 0, 75, and 288 K [67]. Inelastic neutron scattering experiments gave no hint for a noticeable contribution from the CEF at energies up to 18.4 meV [130]. The electronic structure of CePdIn (along with CeNiIn, CeCuIn and CeAuIn) was investigated by X-ray photoelectron spectroscopy [59] and the spectra were analyzed on the basis of the Gunnarsson-Schönhammer model [131–133]. A large hybridization parameter Δ of 177 meV was derived.

The last trivalent compound in the Ce*T*In family is the indide CePtIn. Its physical properties were studied on polycrystalline material and oriented single crystals [26, 125, 128]. Similar to the CePdIn analogue, CePtIn was also classified as a heavy fermion material ($C/T \geq 0.5$ J K^{-2} below 1 K) [134]; however, no magnetic ordering occurs down to 60 mK. The electronic structure of CePtIn was established experimentally on the basis of X-ray photoelectron spectroscopy [71]. The Ce(3d) spectrum was analyzed by the Gunnarsson-Schönhammer model, yielding an energy value of 170 meV for the hybridization between the Ce(4*f*) and the conduction electron band.

Finally we turn to the non-magnetic Kondo compounds, where a further increase of J_{cf} leads to valence fluctuations. This peculiar magnetic behavior preferentially occurs for the Ce*TX* phases with small *T* and *X* atoms and thus smaller cell volumes. CeNiZn shows an almost temperature independent magnetic susceptibility down to 50 K with an absolute value of *ca.* 1.2×10^{-3} emu mol^{-1}, indicating a nearly tetravalent state of cerium [48], i.e., the Ce(4f) shell is practically depleted. In view of the low absolute susceptibility, one can classify CeNiZn as a Pauli paramagnet. The whole susceptibility contribution can be attributed to the conduction electrons.

Susceptibility measurements on CeRhPb also showed Pauli paramagnetism with a comparatively low susceptibility of 2×10^{-3} emu mol^{-1} [77]. In agreement with the non-magnetic 4f^0 ground state, electronic structure calculation revealed a very small 4f contribution in the DOS at the Fermi level.

CeNiAl has the smallest cell volume in the CeNi*X* (*X* = Al, Ga, In) series, and the low susceptibility values indicate mixed valence behavior. No hints for magnetic ordering are evident neither from susceptibility nor from specific heat data [135–137]. α-CeNiGa exhibits comparable behavior of the magnetic susceptibility and the electrical resistivity [90, 91].

The valence fluctuating compound CeNiIn [22, 125, 128] was studied in many combined investigations along with the higher congeners CePdIn and CePtIn. Single crystals of CeNiIn can be grown by the Czochralski technique. Susceptibility, resistivity and specific heat data measured on such single crystals point to significant anisotropic Kondo anomalies. Again, this is a consequence of the anisotropic mixing of Ce(4*f*) and conduction electron states along the *a*, respectively *c* axis.

In the series of *RE*RhIn indides, the cell volume of CeRhIn deviates substantially from the expected lanthanide contraction [64], indicating intermediate valence for the cerium atoms. This is underlined by temperature dependent magnetic susceptibility values which (i) show small absolute values and can (ii) be understood on the basis of the interconfiguration fluctuation model (ICF) proposed by Sales and Wohlleben [138], dividing the whole susceptibility term into Ce^{3+} and Ce^{4+} contributions. The strong reduction of the cerium magnetic moment has also been observed in local susceptibility measurements of ^{140}Ce in *RE*RhIn (*RE* = Y, La, Ce, Gd), using the method of perturbed angular correlation at different temperatures [139]. The elastic properties of CeRhIn were measured on a Czochralski-grown single crystal [24, 140]. The elastic modulus decreases with decreasing temperature (softening) and shows a pronounced minimum around 120 K which is close to the maximum in the magnetic contribution to the specific heat. This maximum is also reproduced in the temperature dependence of the thermopower [141].

Experimental data for the location of the Ce(4f) states were obtained from high-resolution Rh(3*d*)–Ce(4*f*) resonance photoemission spectroscopy [89] in comparison with isotypic CeRhSn. The samples were grown as single crystals via the Czochralski technique. Both compounds show a strong Ce(4f^1) contribution near the Fermi energy and a weak Ce(4f^0) peak, in agreement with strong valence fluctuation behavior. In comparison, the Ce(4*f*) conduction electron hybridization strength in CeRhSn is weaker than that in CeRhIn. These experimental features have been complemented by electronic structure calculations [142].

First hints for intermediate cerium valence in CeRhSn were evident from the course of the cell volume in the series of *RE*RhSn stannides and from susceptibility data [74, 75, 104, 143–149]. CeRhSn and isotypic CeIrSn were then also studied with respect to their thermoelectric behavior. The maxima were observed around 150 K (60 μV K^{-1}) and 300 K (40 μV K^{-1}) for CeRhSn and CeIrSn, respectively [143]. Especially the low temperature properties of CeRhSn were studied in detail and repeatedly reviewed [144–146, 148]. Specific heat measurements showed an enhanced electronic specific heat coefficient of 160 mJ mol^{-1} K^{-2} and resistivity data point to non-Fermi liquid behavior. The

spin fluctuations that were evident from the susceptibility data were confirmed by ^{119}Sn solid state NMR data in the low temperature regime [147].

3.3 Electrical properties

Resistivity data for diverse Ce*TX* intermetallic compounds were measured on polycrystalline as well as single crystalline specimens. The polycrystalline samples often show severe microcracks [e.g., 102 or 106] which irreversibly falsify the absolute values. For this reason often reduced resistivity data are plotted in order to reduce these inconsistencies. For many Ce*TX* compounds only the magnetic contribution (magnetic scattering) is of interest. Therefore the isotypic lanthanum compounds were measured for comparison and the data substracted from the cerium data (see e.g., Ref. [148]).

Usually the RKKY metals show resistivity behavior that can easily be described by a combined Bloch-Grüneisen term in the temperature regime above the magnetic ordering. This model accounts for the residual and spin disorder resistivity, the scattering of conduction electrons on phonons as well as interband scattering processes. Typical examples are CeMgGa [39] or CeCuIn [62]. Another typical feature of the transport properties is the pronounced Kondo minimum observed before the onset of magnetic ordering in the dense Kondo materials. A representative example is CePdIn [127].

The intermediate valence compounds like CeRhIn and CeRhSn show the typical quadratic temperature dependence of the resistivity at low temperatures followed by an almost linear increase. The magnetic scattering of the intermediate valence compounds is expressed through a broad maximum in the high-temperature region [64].

3.4 ^{119}Sn Mössbauer spectroscopy

So far, ^{119}Sn Mössbauer spectroscopy has only been applied to samples of the stannides CeRhSn and CeIrSn and their hydrides [74]. In agreement with the crystal structures, the ^{119}Sn spectra show only one crystallographic tin site for the stannide and the corresponding hydride. The non-cubic site symmetry *m2m* leads to quadrupole splitting. At 78 K the isomer shifts (δ) of CeRhSn (1.84 mm s^{-1}) and CeIrSn (1.76 mm s^{-1}) are very similar and fall in the typical range for intermetallic tin compounds [150, 151]. The hydrides $CeRhSnH_{0.8}$ (δ = 1.87 mm s^{-1}) and $CeIrSnH_{0.7}$ (δ = 1.85 mm s^{-1}) show isomer shifts almost similar to that of the parent ternary stannide, indicating very similar *s* electron density at the tin nuclei [74]. This means that the hydrogenation primarily influences the Ce–*T* bonding and thus the cerium valence, similar to the pair of compounds CeRhSb and $CeRhSbH_{0.2}$ [152].

The crystal field parameters of CeRhSn were derived from the quadrupole splitting parameters ΔE_Q of the ^{155}Gd nuclear ground state in isotypic GdRhSn [149]: B_0^2 = –17.8 K and B_2^2 = –6.4 K.

3.5 High-pressure studies

The first aspect of high-pressure high-temperature studies concerns the synthesis condition. The stannides HP-Ce*T*Sn (*T* = Ni, Pd, Pt) adopt the orthorhombic TiNiSi type structure under ambient conditions and transform to the hexagonal ZrNiAl type upon pressure and temperature treatment [31–33]. Exemplarily, the HP-CePtSn sample was studied by high-temperature, *in-situ* X-ray powder diffraction showing re-transformation to the TiNiSi type normal-pressure modification at around 1170 K [33]. Electronic structure calculations showed a decrease of the covalent binding energy in the high-pressure phase, indicating increasing metallization (delocalization) of all bonds along with a volume contraction. Assuming a rigid band model, bonding in HP-CeNiSn and HP-CePdSn is very similar.

Besides the synthetic studies, only few physical property studies of Ce*TX* intermetallics under high-pressure conditions have been reported. Most of these investigations concerned the resistivity behavior under hydrostatic pressures (see e.g., Ref. [129]).

3.6 Hydrogenation behavior

The coupling constant J_{cf} between the Ce(4f) and the conduction electrons has been discussed on the basis of the Doniach diagram in Chapter 3.2 as the important parameter which governs the magnetic ground state of a given Ce*TX* phase. Hydrogenation of these intermetallics leads to an increase of the unit cell volume along with a decrease in the strength of the J_{cf} parameter. Thus, especially the Ce*TX* phases with intermediate valent cerium are interesting candidates for hydrogen induced changes of the magnetic behavior.

The basic crystallographic data of the Ce*TX*H_x hydrides are listed in Table 3. In addition to these samples, several other Ce*TX* phases have been treated under hydrogen atmosphere. Not all of these samples keep the ZrNiAl structure for the metal substructure of the hydride. CeNiAl

Table 3: Lattice parameters of the hydrogenated Ce*TX* compounds with hexagonal ZrNiAl type structure.

Compound	*a* (pm)	*c* (pm)	*c*/*a*	*V* (nm³)	Volume increase	Magnetic behavior	References
$CeNiInH_{0.3}$	757.4	399.5	0.527	0.1985	2.1 %	< 2 K	[38]
$CeNiInD_{0.48}$	759.19(3)	399.47(2)	0.526	0.1994	2.1 %	n.i.	[61]
$CeNiInH_{0.6}$	762.1	401.4	0.527	0.2019	3.8 %	< 2 K	[38]
$CeNiInH_{0.8}$	761.0	401.4	0.527	0.2013	3.4 %	n.i.	[154]
$CeNiInD_{1.24}$	729.21(3)	426.38(2)	0.585	0.2129	9.0 %	n.i.	[61]
$CeNiInH_{1.6}$	730.3	462.5	0.633	0.2136	9.8 %	T_C = 7 K	[38]
$CeNiInH_{1.8}$	730.8(2)	463.0(1)	0.634	0.2141	11.0 %	T_C = 6.8 K	[161]
$CeNiInH_{1.8}$	729.1	462.4	0.634	0.2129	9.3 %	n.i.	[154]
$CeRhInH_{0.55}$	762.4	407.0	0.534	0.2049	2.3 %	IV	[65]
$CeRhInH_{1.58}$	764.2	410.2	0.537	0.2075	2.3 %	IV	[164]
CePdInH	769.4(2)	419.9(1)	0.546	0.2153	3.5 %	T_N = 3.0 K	[69]
$CePdInD_{1.1}$	770.76(1)	421.72(1)	0.547	0.2170	3.7 %	< 2 K	[156]
$CePtInH_{0.7}$	773.0(3)	411.2(1)	0.532	0.2128	3.2 %	< 2 K	[70]
$CeRhSnH_{0.8}$	755.7(2)	413.6(1)	0.547	0.2046	4.4 %	IV	[74]
$CeIrSnH_{0.7}$	755.7(2)	413.8(1)	0.548	0.2045	4.7 %	IV	[74]

IV, intermediate valence; n.i., not investigated. The volume increase with respect to the parent compounds is also listed. For samples that did not show magnetic ordering the lowest measuring temperature is given.

[37, 55, 153] and CeNiGa [90, 91] transform to an AlB_2 related metal substructure upon hydrogenation. In the present review we focus only on the hydrides with ZrNiAl-type metal substructure.

Besides control of the volumetric hydrogen uptake and the hydrogenation kinetics, the quantity of absorbed hydrogen and the structural consequences are the decisive issues. The latter concern the changes of the unit cell parameters as well as the crystallographic sites occupied by the H atoms. First we discuss the consequence on the lattice parameters. Hydrogenation causes an anisotropic expansion of the unit cell with much larger expansion of the *c* vs. the *a* axes (see data in Table 3). The cell volumes show an increase of up to 11 %, leading to crumbling of the samples.

Since hydrogen has an extremely weak scattering power for X-rays (especially in the neighborhood to the heavy metals of the metal substructure), their position can hardly be detected from X-ray diffraction experiments. First attempts to identify the interstitial sites for the H atoms were of purely geometric nature, analyzing the Ce*TX* substructures with respect to their tetrahedral voids. The possible interstices have been analyzed geometrically for isotypic NdNiIn [154]. In all cases, only part of these voids are filled. The maximum hydrogen content observed corresponds to a composition $CeTXH_{1.8}$.

Several hydrides $CeTXH_x$ have been tested for their thermal stability. Complete release of hydrogen requires temperatures in the range of 700–800 K. Usually the initial Ce*TX* host structure is formed again. The hydrogen desorption can proceed in different steps., which were monitored by differential thermal analyses for selected $CeTXH_x$ samples [154].

The nickel-containing deuterides $CeNiInD_{0.48}$ and $CeNiInD_{1.24}$ were studied by powder neutron diffraction [61]. Both samples show deuterium only on the 4*h* site with occupancy parameters of 0.362 and 0.927 for $CeNiInD_{0.48}$ and $CeNiInD_{1.24}$, respectively. Cutouts of the structures of the host CeNiIn and the deuteride $CeNiInD_{1.24}$ are presented in Fig. 5. D or H atoms fill edge- and face-sharing Ce_3Ni tetrahedra along the *c* axis. The drawing readily reveals the increasing *c*/*a* ratio in the deuteride (16.6 % increase of the *c* axis!). Each D atom has three cerium neighbors at

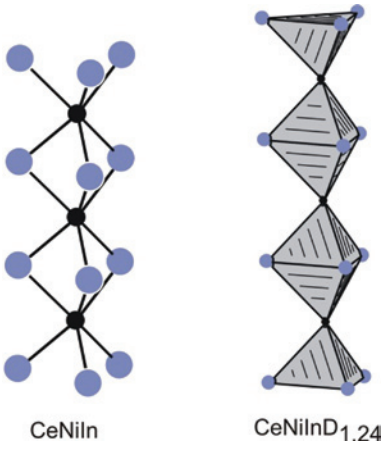

Fig. 5: Comparison of the empty and filled Ce_3Ni tetrahedra in the structures of CeNiIn and $CeNiInD_{1.24}$. Cerium and nickel atoms are drawn as blue and black circles, respectively. Both substructures are drawn with the same enlargement factor.

237 pm and one nickel neighbor at 151 pm. Within such a tetrahedral chain a NiD_2 deuteridonickelate subunit is formed. The face-sharing connectivity of the tetrahedra leads to short D–D distances of 161 pm. The hydrogen substructure has been confirmed by ^{1}H solid state NMR spectroscopy for CeNiInH and $CeNiInH_{1.6}$ samples in the temperature range 140 to 300 K [155].

Besides the $CeNiInD_x$ phases, also $CePdInD_{1.1}$ has been studied in detail by powder neutron diffraction [156] along with other rare earth representatives of that series. This study used a systematic symmetry analyses (including group-subgroup relations) for an exploration of all possible models with different hydrogen positions. The best fit of the diffraction data was obtained for an occupancy of three different Wyckoff sites with deuterium: 50 % on 4*h*, 35 % on 3*g*, and 8 % on 3*f*. Neutron powder diffraction patterns for the $CePdInD_{1.1}$ sample were also collected at 0.8 K. No superstructure reflections indicating long-range magnetic ordering have been detected.

The structural investigations have been accompanied by detailed electronic structure calculations for a concise study of chemical bonding and an evaluation of the magnetic ground states, in comparison of the Ce*TX* and $CeTXH_x$ phases [157–159]. Intermediate-valence CeNiIn was studied along with its hydride. Magnetic calculations of the hydride indicate a finite magnetic moment on the Ce atoms (Ce(4*f*) localization), thus underlining the results of the experimental magnetic property investigations (*vide infra*). Optimization of the hydride structures (cell volumes and *c*/*a* ratios) led to a good agreement with the experimental data. Crystal orbital Hamilton populations underline the Ni–H bonding in the NiH_2 hydridometallate subunits. Another main concern of the calculations were the short H–H distances determined from the neutron diffraction data. All these hydrides violate the so-called Switendick rule [160] (200 pm H–H separation). The first-principles calculations showed a paired and localized electron distribution at the hydrogen sites which is polarized towards the Ce and In atoms, thus reducing the repulsive H–H interactions. Extension of the study to the palladium and platinum containing members showed similar results.

Now we turn to the magnetic and electrical property studies of the hydrides. The most detailed studies were performed on the $CeNiInH_x$ hydrides [36, 38, 161, 162]. Samples with x values of 0.5, 0.6, 0.7, 0.67, 0.75, 1.0, 1.6, and 1.8 have been prepared and studied with respect to the magnetic ground state. Increasing hydrogen content leads to an increase of the cerium magnetic moment, and the hydride with the highest hydrogen content, $CeNiInH_{1.8}$ [161] shows purely trivalent cerium along with a transition to a ferromagnetically ordered state at T_C = 6.8 K. Thus, hydrogenation leads to a drastic decrease of the Kondo interactions and switches the magnetic ground state from intermediate valence to ferromagnetism. This is also expressed in the temperature dependent resistivity data [36]. Specific heat data for a $CeNiInH_{1.6}$ sample show a sharp λ-type transition at T_C, while a moderately hydrogenated sample of composition $CeNiInH_{0.6}$ shows no sign of magnetic ordering [38]. Specific heat measurements on $CeNiInH_{1.8}$ show a significant magnetocaloric effect [163].

CePdIn absorbs one equivalent of hydrogen per formula unit [69]. Cerium remains trivalent in CePdInH. The paramagnetic Curie temperature increases from –42 to –28 K in the sequence CePdIn → CePdInH, indicating decreasing Kondo-type interactions. The Néel temperature increases from 1.65 to 3.0 K. The temperature dependence of the thermoelectric power of CePdInH shows a maximum of 9 μV K^{-1} around 90 K. Polycrystalline $CePdInD_{1.1}$ showed paramagnetic behavior (μ_{exp} = 2.59 μ_B) down to 2 K [156], in contrast to antiferromagnetic CePdInH [69]. This might be a consequence of the slightly different H/D content, leading to domains of different degree of hydrogenation (3 sites were evident from neutron diffraction data) in the polycrystalline samples. The samples without long-range magnetic ordering most likely show strongly delocalized Ce(4*f*) states.

Hydrides $CeRhInH_x$ have been studied for x = 0.55 and 1.58, respectively [65, 164]. The hydride with the larger hydrogen content shows an orthorhombic phase besides the hexagonal one and is transformed to $CeRhInH_{0.55}$ within a short time. Such an instability has rarely been observed for the $CeTXH_x$ phases. $CeRhInH_{0.55}$ shows a slight expansion of the unit cell with respect to CeRhIn. Hydrogenation decreases the occupancy of the rhodium *d* bands (partial charge transfer to hydrogen), thus decreasing the hybridization between the Ce(4*f*) with the Rh(4*d*) states, inducing a shift of the cerium valence towards a nearly trivalent state. The experimental effective magnetic moment of 2.25 μ_B, however, is still reduced when compared with the free ion value of 2.54 μ_B for Ce^{3+}. This behavior is similar to that of the stannides CeRhSn and CeIrSn which form the hydrides $CeRhSnH_{0.8}$ and $CeIrSnH_{0.7}$ [74].

CePtIn renders the hydride $CePtInH_{0.7}$ [70]. Under ambient conditions one observes decomposition of the hydride within a few weeks, leaving the parent compound CePtIn. $CePtInH_{0.7}$ is trivalent without any signs of magnetic ordering down to 2 K. Hydrogenation experiments along with solid state NMR studies were also carried out with CeCuAl [165, 166]. Although hydrogen contents

$CeCuAlH_{0.64}$ and $CeCuAlH_{1.51}$ were reported, structural data on the hydride phases are not available.

Finally some words of caution seem appropriate. The different hydrogenation experiments of the Ce*TX* phases lead to Ce*TX*H_x phases with hydrogen contents up to $x = 1.9$ [167]. Temperature, pressure and grain size of the initial Ce*TX* phases are important parameters that influence the hydride formation. The volumetric measurement of the hydrogen quantity always leaves a small uncertainty for the composition of the final hydride. The neutron diffraction experiments showed different and partial site occupancies for the H atoms. Thus, polycrystalline Ce*TX*H_x samples might have a distribution of domains with different hydrogen content and/or differently occupied interstitial sites. This can easily lead to differences in the magnetic behavior. Especially the different results obtained from the neutron diffraction studies of the nickel indide and palladium indide series are a clear indication that possibly each Ce*TX*H_x phase has its individual hydrogen substructure.

3.7 Solid solutions

As discussed above, distinctly different magnetic ground states occur for the Ce*TX* compounds. Several studies have been devoted to solid solutions in order to investigate transitions between dissimilar ground states or to check whether or not Vegard-type behavior occurs for a given physical property. Examples have been reported for solid solution on all three sites.

Our summary starts with dilution of the cerium magnetic moments through substitution of the rare earth site with non-magnetic lanthanum or yttrium atoms. The evolution of the lattice parameters as a function of cerium-yttrium substitution has been studied in detail for the complete solid solution $Ce_{1-x}Y_xPdAl$ [57]. A distinct anomaly occurs in the range of $0.4 \le x \le 0.6$. These samples show two sets of hexagonal lattice parameters. This indicates coexistence of an yttrium- and a cerium-richer phase, probably due to a miscibility gap. A relation with the high c/a ratio was discussed, however, based on the c/a ratios listed in Table 1 for the whole series of Ce*TX* compounds, these arguments are hardly convincing.

Lanthanum has been substituted for cerium in $Ce_{1-x}La_xPdAl$ in the range of $0 \le x \le 0.2$ [168]. Temperature dependent susceptibility measurements showed a weak decrease of the Néel temperature with increasing lanthanum concentration. Normalization of the susceptibility data to the cerium concentration revealed tri-valent cerium in all samples. An even stronger reduction of the Néel temperature is observed for the solid solution $Ce_{1-x}Y_xPdAl$ in the range $0 \le x \le 0.4$ [169], most likely a consequence of the smaller size of the Y atoms. Again, the cerium remains trivalent in this concentration range. These results have been confirmed through specific heat studies [170].

Dilution of the cerium magnetic moments has also been investigated for $Ce_{1-x}La_xRhSn$ [171, 172]. Both the *a* and *c* lattice parameters increase with increasing lanthanum content. Detailed studies of the thermal and magnetic properties around the critical concentration of $x \approx 0.5$ show spin fluctuation behavior for samples with higher lanthanum content but formation of magnetic clusters (mictomagnetism) towards higher cerium concentration. The origin of a ferromagnetic state at much higher temperatures (around 220 K) is a strange feature. Often iron-contaminated cerium is a reason for such anomalies.

The course of the lattice parameters in the solid solution $Ce_{1-x}La_xPtIn$ [173] shows almost Vegard-type behavior. The cerium magnetic behavior strongly depends on the lanthanum content. Samples in the range $0 \le x \le 0.2$ show dense Kondo behavior which switches to a single-ion Kondo region for $0.3 \le x \le 0.8$. These features are also manifested in resistivity and magnetoresistivity data.

The second group of solid solutions concerns substitution on the transition metal sites. Complete solid solutions are formed in $CeNi_xPd_{1-x}In$ [174] and $CePd_xRh_{1-x}In$ [175]. Starting from CePdIn, the cell volume decreases with increasing nickel, respectively rhodium content (a consequence of the smaller radii of nickel and rhodium). A small degree of palladium-nickel substitution still allows magnetic ordering. The Néel temperature of 1.7 K of CePdIn drops to 1.3 K for a sample of composition $CeNi_{0.2}Pd_{0.8}In$, followed by a break-down of the antiferromagnetic ground state for nickel concentrations larger than 40 %. In the solid solution $CePd_xRh_{1-x}In$ the magnetic ground state changes from antiferromagnetic to intermediate cerium valence. This is similar for $CePd_{1-x}Ni_xAl$ [176–178]. Several samples of this solid solution have been prepared in single crystalline form for specific heat and thermoelectric power measurements.

Solid solutions are also formed in the case of structurally different end members. CeRhSn shows substitution of rhodium by cobalt, nickel, and ruthenium [179]. These studies were performed up to 25 at.-%. The complete solid solution $CeRh_{1-x}Ru_xSn$ was studied recently [180]. The ZrNiAl-type structure is stable up to $CeRh_{0.8}Ru_{0.2}Sn$ and then switches to the monoclinic CeRuSn type [181, 182]. Cerium is in an intermediate valence state over the entire concentration range. This

is evident from magnetic susceptibility studies evaluated with the interconfiguration fluctuation (ICF) model introduced by Sales and Wohlleben, as well as from XANES data. The situation is similar for $CeRh_{1-x}Pd_xSn$ [183] and $CeRu_{1-x}Ni_xAl$ [184] which show the ZrNiAl-type structure for $0 \le x \le 0.8$ and $0.9 \le x \le 1$, respectively. Special cases are $CeRu_{1-x}Pd_xSn$ [183] and $CeRu_{1-x}Ni_xSn$ [185]. CeRuSn allows only for tiny substitutions of ruthenium on the one side, and the end members CePdSn and CeNiSn crystallize with the orthorhombic TiNiSi type on the other. Thus one observes formation of the ZrNiAl-type phases only for $0.1 \le x \le 0.7$ and $0.1 \le x \le 0.4$, respectively. In all these regimes, the ZrNiAl-type phases show intermediate cerium valence.

Substitution on the transition metal positions is also possible with another p element. Two recent examples concern the solid solutions $CeRh_{1-x}Ge_xIn$ ($0.1 \le x \le 0.3$) [186] and $CePd_{1-x}Ge_xIn$ ($0.1 \le x \le 0.4$) [187]. Single crystal diffraction data revealed Rh/Ge respectively Pd/Ge mixing only on the 2*d* sites, i.e., within the trigonal prisms formed by the Ce atoms. For the $CeRh_{1-x}Ge_xIn$ series, with increasing germanium content the intermediate cerium valence changes to a localized Ce(4*f*) state. A change of the magnetic ground state is also observed for the palladium based series. With increasing germanium content the coherent Kondo state of CePdIn vanishes gradually.

The last two solid solutions concern substitutions on the *X* sites. Sn atoms of CeRhSn have gradually been replaced by indium [188]. The course of the magnetic susceptibility data and the electric transport properties showed a transition from a non-Fermi liquid state to intermediate valence behavior. In the solid solution $CeAuIn_{1-x}Mg_x$ [189] one observes a direct break-down of magnetic ordering when indium is substituted by magnesium. Over the whole range of solid solutions one observes only very small changes in the lattice parameters.

4 Summary

The ZrNiAl type Ce*TX* intermetallics exhibit many different facets of magnetic ground states ranging from antiferromagnetic ordering to pronounced valence fluctuation. The present review presents the results of the detailed studies of physical properties which have been performed over the last thirty years and thus manifests the topicality of this research field. Especially solid solutions and hydrogenation products of these Ce*TX* intermetallics are still in the focus of solid state physics and chemistry research in order to elucidate structure-property relationships.

Acknowledgments: This work was supported by the Deutsche Forschungsgemeinschaft.

References

[1] P. Villars, K. Cenzual, *Pearson's Crystal Data: Crystal Structure Database for Inorganic Compounds* (release 2014/15), ASM International®, Materials Park, Ohio (USA) **2014**.
[2] A. Szytuła, J. Leciejewicz, *Handbook of Crystal Structures and Magnetic Properties of Rare Earth Intermetallics*, CRC Press, Boca Raton, **1994**.
[3] W. Suski, *J. Magn*. **1999**, *4*, 102.
[4] G. R. Stewart, *Rev. Mod. Phys*. **2006**, *78*, 743.
[5] R. Settai, T. Takeuchi, Y. Ōnuki, *J. Phys. Soc. Jpn*. **2007**, *76*, 051003.
[6] H. von Löhneysen, A. Rosch, M. Vojta, P. Wölfle, *Rev. Mod. Phys*. **2007**, *79*, 1015.
[7] P. Gegenwart, Q. Si, F. Steglich, *Nat. Phys*. **2008**, *4*, 186.
[8] O. Stockert, S. Kirchner, F. Steglich, Q. Si, *J. Phys. Soc. Jpn*. **2012**, *81*, 011001.
[9] S. F. Matar, *Progr. Solid State Chem*. **2013**, *41*, 55.
[10] S. Gupta, K. G. Suresh, *J. Alloys Compd*. **2015**, *618*, 562.
[11] R. Pöttgen, Th. Gulden, A. Simon, *GIT Labor Fachz*. **1999**, *43*, 133.
[12] B. J. Gibson, A. Das, R. K. Kremer, R.-D. Hoffmann, R. Pöttgen, *J. Phys.: Condens. Matter* **2002**, *14*, 5173.
[13] J. Emsley, *The Elements*, Oxford University Press, Oxford, **1999**.
[14] J. D. Corbett, A. Simon, *Inorg. Synth*. **1983**, *22*, 15.
[15] R. Pöttgen, D. Johrendt, *Intermetallics*, De Gruyter, Berlin, **2014**.
[16] D. Kußmann, R.-D. Hoffmann, R. Pöttgen, *Z. Anorg. Allg. Chem*. **1998**, *624*, 1727.
[17] R. Pöttgen, A. Lang, R.-D. Hoffmann, B. Künnen, G. Kotzyba, R. Müllmann, B. D. Mosel, C. Rosenhahn, *Z. Kristallogr*. **1999**, *214*, 143.
[18] V. I. Zaremba, U. Ch. Rodewald, R. Pöttgen, *Z. Anorg. Allg. Chem*. **2005**, *631*, 1065.
[19] M. G. Kanatzidis, R. Pöttgen, W. Jeitschko, *Angew. Chem. Int. Ed*. **2005**, *44*, 6996.
[20] R. Movshovich, J. M. Lawrence, M. F. Hundley, J. Neumeier, J. D. Thompson, A. Lacerda, Z. Fisk, *Phys. Rev. B* **1996**, *53*, 5465.
[21] H. Sadamura, H. Fujii, T. Okamoto, *IEEE Transl. J. Magn. Jpn*. **1985**, *1*, 810.
[22] H. Fujii, T. Inoue, Y. Andoh, T. Takabatake, K. Satoh, Y. Maeno, T. Fujita, J. Sakurai, Y. Yamaguchi, *Phys. Rev. B* **1989**, *39*, 6840.
[23] H. Fujii, T. Takabatake, Y. Andoh, *J. Alloys Compd*. **1992**, *181*, 111.
[24] H. Higaki, I. Ishii, M.-S. Kim, D. Hirata, T. Takabatake, T. Suzuki, *Physica B* **2005**, *359–361*, 136.
[25] M. Klicpera, J. Pospíšil, A. Rudajevová, A. Hoser, P. Javorský, *J. Cryst. Growth* **2014**, *394*, 61.
[26] M. Klicpera, P. Javorský, *Mater. Res. Express* **2014**, *1*, 016301.
[27] H. Huppertz, *Z. Kristallogr*. **2004**, *219*, 330.
[28] D. Walker, M. A. Carpenter, C. M. Hitch, *Am. Mineral*. **1990**, *75*, 1020.
[29] D. Walker, *Am. Mineral*. **1991**, *76*, 1092.
[30] D. C. Rubie, *Phase Trans*. **1999**, *68*, 431.

[31] J. F. Riecken, G. Heymann, W. Hermes, U. Ch. Rodewald, R.-D. Hoffmann, H. Huppertz, R. Pöttgen, *Z. Naturforsch*. **2008**, *63b*, 695.
[32] G. Heymann, J. F. Riecken, S. Rayaprol, S. Christian, R. Pöttgen, H. Huppertz, *Z. Anorg. Allg. Chem*. **2007**, *633*, 77.
[33] J. F. Riecken, G. Heymann, T. Soltner, R.-D. Hoffmann, H. Huppertz, D. Johrendt, R. Pöttgen, *Z. Naturforsch*. **2005**, *60b*, 821.
[34] B. Tanguy, J.-L. Soubeyroux, M. Pezat, J. Portier, P. Hagenmuller, *Mater. Res. Bull*. **1976**, *11*, 1441.
[35] S. Pechev, B. Chevalier, M. Khrussanova, M. Terzieva, J. L. Bobet, B. Darriet, P. Peshev, *J. Alloys Compd*. **1997**, *259*, 24.
[36] B. Chevalier, M. Pasturel, J.-L. Bobet, R. Decourt, J. Etourneau, O. Isnard, J. Sanchez Marcos, J. Rodriguez Fernandez, *J. Alloys Compd*. **2004**, *383*, 4.
[37] M. Stange, V. Paul-Boncour, M. Latroche, A. Percheron-Guégan, O. Isnard, V. A. Yartys, *J. Alloys Compd*. **2005**, *404–406*, 144.
[38] K. Shashikala, A. Sathyamoorthy, P. Raj, S. K. Dhar, S. K. Malik, *J. Alloys Compd*. **2007**, *437*, 7.
[39] R. Kraft, R. Pöttgen, D. Kaczorowski, *Chem. Mater*. **2003**, *15*, 2998.
[40] R. Kraft, M. Valldor, R. Pöttgen, *Z. Naturforsch*. **2003**, *58b*, 827.
[41] R. Kraft, M. Valldor, D. Kurowski, R.-D. Hoffmann, R. Pöttgen, *Z. Naturforsch*. **2004**, *59b*, 513.
[42] R. Kraft, R. Pöttgen, *Z. Naturforsch*. **2005**, *60b*, 265.
[43] Th. Fickenscher, R.-D. Hoffmann, R. Kraft, R. Pöttgen, *Z. Anorg. Allg. Chem*. **2002**, *628*, 667.
[44] A. Iandelli, *J. Alloys Compd*. **1994**, *203*, 137.
[45] C. Geibel, U. Klinger, M. Weiden, B. Buschinger, F. Steglich, *Physica B* **1997**, *237–238*, 202.
[46] T. Fickenscher, R. Pöttgen, *J. Solid State Chem*. **2001**, *161*, 67.
[47] D. Johrendt, G. Kotzyba, H. Trill, B. D. Mosel, H. Eckert, Th. Fickenscher, R. Pöttgen, *J. Solid State Chem*. **2002**, *164*, 201.
[48] W. Hermes, R. Mishra, U. Ch. Rodewald, R. Pöttgen, *Z. Naturforsch*. **2008**, *63b*, 537.
[49] A. Iandelli, *J. Alloys Compd*. **1992**, *182*, 87.
[50] W. Hermes, R. Mishra, H. Müller, D. Johrendt, R. Pöttgen, *Z. Anorg. Allg. Chem*. **2009**, *635*, 660.
[51] T. Fickenscher, R.-D. Hoffmann, R. Mishra, R. Pöttgen, *Z. Naturforsch*. **2002**, *57b*, 275.
[52] R. Mishra, R. Pöttgen, R.-D. Hoffmann, D. Kaczorowski, H. Piotrowski, P. Mayer, C. Rosenhahn, B. D. Mosel, *Z. Anorg. Allg. Chem*. **2001**, *627*, 1283.
[53] M. Johnscher, F. Tappe, O. Niehaus, R. Pöttgen, *Z. Naturforsch*. **2015**, *70b*, 197.
[54] A. E. Dwight, M. H. Mueller, R. A. Conner Jr., J. W. Downey, H. Knott, *Trans. Met. Soc. AIME* **1968**, *242*, 2075.
[55] J.-L. Bobet, B. Chevalier, B. Darriet, M. Nakhl, F. Weill, J. Etourneau, *J. Alloys Compd*. **2001**, *317–318*, 67.
[56] B. Xue, H. Schwer, F. Hulliger, *Acta Crystallogr.* **1994**, *C50*, 338.
[57] J. Prchal, H. Kitazawa, O. Suzuki, *J. Alloys Compd*. **2007**, *437*, 117.
[58] Y. P. Yarmolyuk, Y. Grin, E. I. Gladyshevskii, *Dopov. Akad. Nauk Ukr. RSR Ser. A* **1979**, 771.
[59] A. Szytuła, B. Penc, Ł. Gondek, *Acta Phys. Polon. A* **2007**, *111*, 475.
[60] M. Pustovoychenko, Yu. Tyvanchuk, I. Hayduk, Ya. Kalychak, *Intermetallics* **2010**, *18*, 929.
[61] V. A. Yartys, R. V. Denys, B. C. Hauback, H. Fjellvåg, I. I. Bulyk, A. B. Riabov, Ya. M. Kalychak, *J. Alloys Compd*. **2002**, *330–332*, 132.
[62] A. Szytuła, D. Kaczorowski, M. Kalychak, B. Penc, Yu. Tyvanchuk, A. Winiarski, *J. Phys. Chem. Solids* **2008**, *69*, 2416.
[63] A. Szytuła, Yu. Tyvanchuk, T. Jaworska-Gołab, A. Zarzycki, Ya. Kalychak, Ł. Gondek, N. Stüsser, *Chem. Met. Alloys* **2008**, *1*, 97.
[64] D. T. Adroja, S. K. Malik, B. D. Padalia, R. Vijayaraghavan, *Phys. Rev. B* **1989**, *39*, 4831.
[65] P. Raj, A. Sathyamoorthy, K. Shashikala, C. R. Venkateswara Rao, D. Kundaliya, S. K. Malik, *J. Alloys Compd*. **2002**, *345*, L1.
[66] A. I. Tursina, S. N. Nesterenko, Yu. D. Seropegin, *Acta Crystallogr.* **2004**, *E60*, i64.
[67] Ł. Gondek, A. Szytuła, D. Kaczorowski, K. Nenkov, *Solid State Commun*. **2007**, *142*, 556.
[68] E. Brück, M. van Sprang, J. C. P. Klaasse, F. R. de Boer, *J. Appl. Phys*. **1988**, *63*, 3417.
[69] B. Chevalier, A. Wattiaux, J.-L. Bobet, *J. Phys.: Condens. Matter* **2006**, *18*, 1743.
[70] W. Hermes, U. Ch. Rodewald, B. Chevalier, R. Pöttgen, *Solid State Sci*. **2007**, *9*, 874.
[71] A. Jezierski, B. Penc, A. Szytuła, A. Winiarski, *Acta Phys. Polon. A* **2012**, *122*, 212.
[72] D. Rossi, R. Ferro, V. Contardi, R. Marazza, *Z. Metallkd*. **1977**, *68*, 493.
[73] R. Ferro, R. Marazza, G. Rambaldi, *Z. Metallkd*. **1974**, *65*, 40.
[74] B. Chevalier, C. P. Sebastian, R. Pöttgen, *Solid State Sci*. **2006**, *8*, 1000.
[75] T. Schmidt, D. Johrendt, C. P. Sebastian, R. Pöttgen, K. Łątka, R. Kmieć, *Z. Naturforsch*. **2005**, *60b*, 1036.
[76] P. Salamakha, O. Sologub, J. K. Yakinthos, Ch. D. Routsi, *J. Alloys Compd*. **1998**, *265*, L1.
[77] L. D. Gulay, D. Kaczorowski, A. Szajak, A. Pietraszko, *J. Phys. Chem. Solids* **2008**, *69*, 1934.
[78] W. Hermes, S. Rayaprol, R. Pöttgen, *Z. Naturforsch*. **2007**, *62b*, 901.
[79] R. Marazza, D. Mazzone, P. Riani, G. Zanicchi, *J. Alloys Compd*. **1995**, *220*, 241.
[80] P. I. Krypyakevich, V. Ya. Markiv, E. V. Melnyk, *Dopov. Akad. Nauk. Ukr. RSR Ser. A* **1967**, 750.
[81] M. F. Zumdick, R.-D. Hoffmann, R. Pöttgen, *Z. Naturforsch*. **1999**, *54b*, 45.
[82] S. Rundqvist, F. Jellinek, *Acta Chem. Scand*. **1959**, *13*, 425.
[83] E. Parthé, L. Gelato, B. Chabot, M. Penzo, K. Cenzual, R. Gladyshevskii, TYPIX–*Standardized Data and Crystal Chemical Characterization of Inorganic Structure Types*, *Gmelin Handbook of Inorganic and Organometallic Chemistry*, 8th edition, Springer, Berlin, **1993**.
[84] M. F. Zumdick, R. Pöttgen, *Z. Kristallogr*. **1999**, *214*, 90.
[85] J. Donohue, *The Structures of the Elements*, Wiley, New York, **1974**.
[86] H. H. Hill in *Plutonium and Other Actinides, Nuclear Materials Series, AIME*, Vol. 17 (Ed.: W. N. Mines), **1970**, pp. 2.
[87] R. P. Singh, *J. Magnesium Alloys* **2014**, *2*, 349.
[88] S. F. Matar, J. Etourneau, R. Pöttgen, *Solid State Sci*., in press.
[89] K. Shimada, H. Namatame, M. Taniguchi, M. Higashiguchi, S.-I. Fujimori, Y. Saitoh, A. Fujimori, M. S. Kim, D. Hirata, T. Takabatake, *Physica B* **2006**, *378–380*, 791.

[90] B. Chevalier, J.-L. Bobet, E. Gaudin, M. Pasturel, J. Etourneau, *J. Solid State Chem*. **2002**, *168*, 28.
[91] B. Chevalier, J. Sanchez Marcos, J. Rodriguez Fernandez, M. Pasturel, F. Weill, *Phys. Rev. B* **2005**, *71*, 214437.
[92] M. A. Ruderman, C. Kittel, *Phys. Rev*. **1954**, *96*, 99.
[93] T. Kasuya, *Prog. Theor. Phys*. **1956**, *16*, 45.
[94] K. Yosida, *Phys. Rev*. **1957**, *106*, 893.
[95] J. Kondo, *Prog. Theor. Phys*. **1964**, *32*, 37.
[96] B. Cornut, B. Coqblin, *Phys. Rev. B* **1972**, *5*, 4541.
[97] S. Doniach, *Physica B* **1977**, *91*, 231.
[98] J. R. Iglesias, C. Lacroix, B. Coqblin, *Phys. Rev. B* **1997**, *56*, 11820.
[99] Y.-F. Yang, Z. Fisk, H.-O. Lee, J. D. Thompson, D. Pines, *Nature* **2008**, *454*, 611.
[100] D. Rossi, D. Mazzone, R. Marazza, R. Ferro, *Z. Anorg. Allg. Chem*. **1983**, *507*, 235.
[101] H. Oesterreicher, *J. Less-Common Met*. **1973**, *30*, 225.
[102] P. Javorský, L. Havela, V. Sechovský, H. Michor, K. Jurek, *J. Alloys Compd*. **1998**, *264*, 38.
[103] B. Chevalier, J.-L. Bobet, *Intermetallics* **2001**, *9*, 835.
[104] Ch. D. Routsi, J. K. Yakinthos, H. Gamari-Seale, *J. Magn. Magn. Mater*. **1992**, *117*, *79*.
[105] R. K. Singhal, N. L. Saini, K. B. Garg, J. Kanski, L. Ilver, P. O. Nilsson, R. Kumar, L. C. Gupta, *J. Phys.: Condens. Matter* **1993**, *5*, 4013.
[106] H. R. Pleger, E. Bruck, E. Braun, F. Oster, A. Freimuth, B. Politt, B. Roden, D. Wohlleben, *J. Magn. Magn. Mater*. **1987**, *63 & 64*, 107.
[107] Ł. Gondek, A. Szytuła, B. Penc, J. Hernandez-Velasco, A. Zygmunt, *J. Magn. Magn. Mater*. **2003**, *262*, L177.
[108] L. Gondek, A. Szytula, S. Baran, J. Hernadez-Velasco, *J. Magn. Magn. Mater*. **2004**, *272–276*, e443.
[109] A. Oyamada, T. Kaibuchi, M. Nishiyama, T. Itou, S. Maegawa, Y. Isikawa, A. Dönni, H. Kitazawa, *J. Phys.: Conf. Ser*. **2011**, *320*, 012067.
[110] V. Fritsch, N. Bagrets, G. Goll, W. Kittler, M. J. Wolf, K. Grube, C.-L. Huang, H. von Löhneysen, *Phys. Rev. B* **2014**, *89*, 054416.
[111] M. A. Romero, A. A. Aligia, J. G. Sereni, *J. Phys.: Condens. Matter* **2014**, *26*, 025602.
[112] H. Kitazawa, A. Matsushita, T. Matsumoto, T. Suzuki, *Physica B* **1994**, *199 & 200*, 28.
[113] W. Głogowski, J. Goraus, A. Ślebarski, *Mater. Sci. Poland* **2008**, *26*, 729.
[114] S. Woitschach, O. Stockert, M. M. Koza, V. Fritsch, H. von Löhneysen, F. Steglich, *Phys. Stat. Sol. B* **2013**, *250*, 468.
[115] A. Dönni, G. Ehlers, H. Maletta, P. Fischer, H. Kitazawa, M. Zolliker, *J. Phys.: Condens. Matter* **1996**, *8*, 11213.
[116] L. Keller, A. Dönni, H. Kitazawa, B. van den Brandt, *Appl. Phys. A* **2002**, *74*, S686.
[117] K. Prokeš, P. Manuel, D. T. Adroja, H. Kitazawa, T. Goto, Y. Isikawa, *Physica B* **2006**, *385–386*, 359.
[118] M. Nishiyama, A. Oyamada, S. Maegawa, T. Goto, H. Kitazawa, *J. Phys.: Condens. Matter* **2003**, *15*, S2267.
[119] A. Oyamada, S. Maegawa, M. Nishiyama, H. Kitazawa, Y. Isikawa, *Phys. Rev. B* **2008**, *77*, 064432.
[120] S. Hane, T. Goto, T. Abe, Y. Isikawa, *Physica B* **2000**, *281 & 282*, 391.
[121] S. Akamaru, Y. Isikawa, T. Kuwai, T. Mizushima, J. Sakurai, Y. Uwatoko, *Physica B* **2002**, *312–313*, 466.
[122] T. Goto, S. Hane, K. Uemo, T. Takabatake, Y. Isikawa, *J. Phys. Chem. Solids* **2002**, *63*, 1159.
[123] K. Prokeš, P. Manuel, D. T. Adroja, H. Kitazawa, T. Goto, Y. Isikawa, *J. Magn. Magn. Mater*. **2007**, *310*, e28.
[124] Y. Maeno, M. Takahashi, T. Fujita, Y. Uwatoko, H. Fujii, T. Okamoto, *Jpn. J. Appl. Phys*. **1987**, *Suppl. 26–3*, 545.
[125] H. Fujii, Y. Uwatoko, M. Akayama, K. Satoh, Y. Maeno, T. Fujita, J. Sakurai, H. Kamimura, T. Okamoto, *Jpn. J. Appl. Phys*. **1986**, *Suppl. 26–3*, 549.
[126] K. Satoh, Y. Maeno, T. Fujita, Y. Uwatoko, H. Fujii, *J. Phys. Colloque C8*, **1988**, *49*, 779.
[127] H. Fujii, M. Nagasawa, H. Kawanaka, T. Inoue, T. Takabatake, *Physica B* **1990**, *165 & 166*, 435.
[128] K. Satoh, T. Fujita, Y. Maeno, Y. Uwatoko, H. Fujii, *J. Phys. Soc. Jpn*. **1990**, *59*, 692.
[129] M. Kurisu, T. Takabatake, H. Fujii, *J. Magn. Magn. Mater*. **1990**, *90 & 91*, 469.
[130] Ł. Gondek, J. Czub, A. Szytuła, Z. Izaola, E. Kemner, *Solid State Commun*. **2009**, *149*, 1596.
[131] J. C. Fuggle, F. U. Hillebrecht, Z. Zołnierek, R. Lässer, Ch. Freiburg, O. Gunnarsson, K. Schönhammer, *Phys. Rev. B* **1983**, *27*, 7330.
[132] O. Gunnarsson, K. Schönhammer, *Phys. Rev. B* **1983**, *28*, 4315.
[133] N. Witkowski, F. Bertran, D. Malterre, *J. Electr. Spectr. Rel. Phen*. **2001**, *117–118*, 371.
[134] T. Fujita, K. Satoh, Y. Maeno, Y. Uwatoko, H. Fujii, *J. Magn. Magn. Mater*. **1988**, *76 & 77*, 133.
[135] L. Menon, A. Agarwal, S. K. Malik, *Physica B* **1997**, *230–232*, 201.
[136] P. Javorský, A. Chernyavsky, V. Sechovský, *Physica B* **2000**, *281 & 282*, 71.
[137] N. C. Tuan, V. Sechovský, M. Diviš, P. Svoboda, H. Nakotte, F. R. de Boer, N. H. Kim-Ngan, *J. Appl. Phys*. **1993**, *73*, 5677.
[138] B. C. Sales, D. K. Wohlleben, *Phys. Rev. Lett*. **1975**, *35*, 1240.
[139] M. N. Nyayate, S. H. Devare, S. K. Malik, D. T. Adroja, H. G. Devare, *Phys. Lett. A* **1990**, *151*, 547.
[140] H. Higaki, I. Ishii, D. Hirata, M.-S. Kim, T. Takabatake, T. Suzuki, *J. Phys. Soc. Jpn*. **2006**, *75*, 024709.
[141] A. M. Strydom, S. Paschen, F. Steglich, *Physica B* **2006**, *378–380*, 793.
[142] M. Gamża, A. Ślebarski, H. Rosner, *Eur. Phys. J. B* **2009**, *67*, 483.
[143] Y. Bando, T. Suemitsu, K. Takagi, H. Tokushima, Y. Echizen, K. Katoh, K. Uemo, Y. Maeda, T. Takabatake, *J. Alloys Compd*. **2000**, *313*, 1.
[144] A. Ślebarski, M. B. Maple, E. J. Freeman, C. Sirvent, M. Radłowska, A. Jezierski, E. Granado, Q. Huang, J. W. Lynn, *Philos. Mag. B* **2002**, *82*, 943.
[145] M. S. Kim, Y. Echizen, K. Umeo, S. Kobayashi, M. Sera, P. S. Salamakha, O. L. Sologub, T. Takabatake, X. Chen, T. Tayama, T. Sakakibara, M. H. Jung, M. B. Maple, *Phys. Rev. B* **2003**, *68*, 054416.
[146] P.-C. Ho, V. S. Zapf, A. Ślebarski, M. B. Maple, *Phil. Mag*. **2004**, *84*, 2119.
[147] H. Tou, M. S. Kim, T. Takabatake, M. Sera, *Phys. Rev. B* **2004**, *70*, 100407.
[148] A. Ślebarski, *J. Low Temp. Phys*. **2007**, *147*, 147.
[149] K. Łątka, R. Kmieć, A. W. Pacyna, R. Pöttgen, *J. Magn. Magn. Mater*. **2008**, *320*, L18.
[150] R. Mishra, R. Pöttgen, R.-D. Hoffmann, H. Trill, B. D. Mosel, H. Piotrowski, M. F. Zumdick, *Z. Naturforsch*. **2001**, *56b*, 589.

[151] R. Pöttgen, *Z. Naturforsch*. **2006**, *61b*, 677.
[152] B. Chevalier, R. Decourt, B. Heying, F. M. Schappacher, U. Ch. Rodewald, R.-D. Hoffmann, R. Pöttgen, R. Eger, A. Simon, *Chem. Mater*. **2007**, *19*, 28.
[153] K. Shashikala, A. Sathyamoorthy, P. Raj, W. B. Yelon, S. K. Malik, *J. Alloys Compd*. **2007**, *438*, 84.
[154] I. I. Bulyk, V. A. Yartys, R. V. Denys, Ya. M. Kalychak, I. R. Harris, *J. Alloys Compd*. **1999**, *284*, 256.
[155] K. Ghoshray, B. Bandyopadhyay, M. Sen, A. Ghoshray, N. Chatterjee, *Phys. Rev. B* **1993**, *47*, 8277.
[156] Ł. Gondek, K. Koźlak, J. Czub, J. Przewoźnik, A. Kupczak, W. Sikora, A. Hoser, P. Prokhenko, N. Tsapatsaris, *Acta Mater*. **2014**, *81*, 161.
[157] S. F. Matar, B. Chevalier, V. Eyert, J. Etourneau, *Solid State Sci*. **2003**, *5*, 1385.
[158] P. Vajeeston, P. Ravindran, R. Vidya, A. Kjekshus, H. Fjellvåg, V. A. Yartys, *Phys. Rev. B* **2003**, *67*, 014101.
[159] P. Vajeeston, P. Ravindran, H. Fjellvåg, A. Kjekshus, *Phys. Rev. B* **2004**, *70*, 014107.
[160] A. C. Switendick, *Z. Phys. Chem. B* **1979**, *117*, 89.
[161] B. Chevalier, M. L. Kahn, J.-L. Bobet, M. Pasturel, J. Etourneau, *J. Phys.: Condens. Matter* **2002**, *14*, L365.
[162] M. Sen, S. Giri, K. Ghoshray, B. Bandyopadhyay, A. Ghoshray, N. Chatterjee, *Solid State Commun*. **1994**, *89*, 327.
[163] J. Sanchez Marcos, J. Rodriguez Fernandez, B. Chevalier, J.-L. Bobet, *Physica B* **2006**, *378–380*, 799.
[164] S. K. Malik, D. Kundaliya, A. Sathyamoorthy, K. Shashikala, P. Raj, V. V. Krishnamurthy, *J. Appl. Phys*. **2003**, *93*, 7834.
[165] B. Bandyopadhyay, K. Ghoshray, A. Ghoshray, N. Chatterjee, *Phys. Rev. B* **1988**, *38*, 8455.
[166] B. Bandyopadhyay, K. Ghoshray, A. Ghoshray, N. Chatterjee, *Phys. Rev. B* **1992**, *46*, 2912.
[167] J.-L. Bobet, M. Pasturel, B. Chevalier, *Intermetallics* **2006**, *14*, 544.
[168] H. Kitazawa, N. Tsujii, O. Suzuki, J. Prchal, M. Imai, A. Dönni, *Physica B* **2008**, *403*, 890.
[169] H. Kitazawa, J. Prchal, N. Tsujii, M. Imai, G. Kido, *Physica B* **2006**, *378–380*, 803.
[170] P. Čermák, H. Kitazawa, J. Prchal, P. Javorský, *J. Phys.: Condens. Matter* **2010**, *22*, 126002.
[171] A. Ślebarski, M. Radłowska, T. Zawada, M. B. Maple, A. Jezierski, A. Zygmunt, *Phys. Rev. B* **2002**, *66*, 104434.
[172] A. Ślebarski, A. Czopnik, A. Zygmunt, T. Zawada, *J. Phys.: Condens. Matter* **2004**, *16*, 4897.
[173] F. C. Ragel, P. de V. du Plessis, A. M. Strydom, *J. Phys.: Condens. Matter* **2009**, *21*, 046008.
[174] M. Klicpera, P. Javorský, E. Šantavá, *J. Phys.: Condens. Matter* **2013**, *25*, 245501.
[175] E. Brück, H. Nakotte, K. Bakker, F. R. de Boer, P. F. de Châtel, J.-Y. Li, J. P. Kuang, F.-M. Yang, *J. Alloys Compd*. **1993**, *200*, 79.
[176] Y. Isikawa, T. Kuwai, T. Mizushima, T. Abe, G. Nakamura, J. Sakurai, *Physica B* **2000**, *281 & 282*, 365.
[177] D. Huo, T. Kuwai, T. Mizushima, Y. Isikawa, J. Sakurai, *Physica B* **2002**, *312–313*, 232.
[178] V. Fritsch, C.-H. Huang, N. Bagrets, K. Grube, S. Schumann, H. von Löhneysen, *Phys. Stat. Sol. B* **2013**, *250*, 506.
[179] Y. Echizen, K. Yamane, T. Takabatake, *Physica B* **2003**, *329–333*, 522.
[180] O. Niehaus, P. M. Abdala, J. F. Riecken, F. Winter, B. Chevalier, *Z. Naturforsch*. **2013**, *68b*, 960.
[181] J. F. Riecken, W. Hermes, B. Chevalier, R.-D. Hoffmann, F. M. Schappacher, R. Pöttgen, *Z. Anorg. Allg. Chem*. **2007**, *633*, 1094.
[182] S. F. Matar, J. F. Riecken, B. Chevalier, R. Pöttgen, V. Eyert, *Phys. Rev. B* **2007**, *76*, 174434.
[183] O. Niehaus, P. M. Abdala, R. Pöttgen, *Z. Naturforsch*. **2015**, *70b*, 253.
[184] O. Niehaus, U. Ch. Rodewald, P. M. Abdala, R. S. Touzani, B. P. T. Fokwa, O. Janka, *Inorg. Chem*. **2014**, *53*, 2471.
[185] O. Niehaus, P. M. Abdala, R. S. Touzani, B. P. T. Fokwa, R. Pöttgen, *Solid State Sci*. **2015**, *40*, 36.
[186] P. Wiśniewski, V. I. Zaremba, A. Ślebarski, D. Kaczorowski, *Intermetallics* **2015**, *56*, 101.
[187] D. Gnida, N. Dominyuk, V. Zaremba, D. Kazorowski, *J. Alloys Compd*. **2015**, *622*, 681.
[188] A. Ślebarski, M. Fijałkowski, J. Goraus, *J. Phys.: Condens. Matter* **2012**, *24*, 0125601.
[189] S. Rayaprol, B. Heying, R. Pöttgen, *Z. Naturforsch*. **2006**, *61b*, 495.